Undrained capacity of circular shallow foundations on two-layer clays under combined VHMT loading

He, Pengpeng; Newson, Tim

Published in:
Canadian Geotechnical Journal

DOI:
10.1139/cgj-2019-0814

Publication date:
2022

Document Version
Peer reviewed version

He, P & Newson, T 2022, 'Undrained capacity of circular shallow foundations on two-layer clays under combined VHMT loading', Canadian Geotechnical Journal, vol. 59, no. 8, pp. 1523-1526. https://doi.org/10.1139/cgj-2019-0814 ©2022 Canadian Science Publishing

Undrained capacity of circular shallow foundations on two-layer clays under combined VHMT loading

(Clean Version)

Author 1:

Pengpeng He, Ph.D. candidate

Geotechnical Research Centre, Department of Civil & Environmental Engineering, Western University, London, Canada

Email: phe27@uwo.ca

Author 2:

Tim Newson, Ph.D., Associate Prof.

Geotechnical Research Centre, Department of Civil & Environmental Engineering, Western University, London, Canada

Email: tnewson@eng.uwo.ca

Corresponding author:

Tim Newson, Ph.D., Associate Prof.

Geotechnical Research Centre, Department of Civil & Environmental Engineering, Western University, London, Canada

Email: tnewson@eng.uwo.ca

Tel: (+1) 519-850-2973; Fax: 519-661-3942

Word count: 1890 (texts) + 3*250 = 2640 (3 figures, including captions but excluding this title page)

Abstract: Wind turbines are typically designed based on fatigue and serviceability limit states, but still require an accurate assessment of bearing capacity. Overconsolidated clay deposits in Canada often have a thin layer of crust with a relatively high undrained shear strength developed from weathering, desiccation, and geo-chemical processes. However, existing design methods only assess the bearing capacity using effective area and inclination factor without consideration of surficial crusts. This paper studies the undrained VHMT (vertical, horizontal, moment and torsional) failure envelope of circular foundations founded on a surficial crust underlain by a uniform soil with a zero-tension interface condition using finite element analysis. An analytical expression for the VHMT failure envelope is derived.

Keywords: Surficial crust; circular foundation; zero-tension interface; failure envelope; finite element analysis.

Introduction

The shallow foundations of onshore and offshore foundations, such as wind turbines and transmission towers, are often subjected to combined vertical, horizontal, moment and torsional (VHMT) loads. Traditionally, the bearing capacity design of these shallow foundations is based on classical solutions for the uniaxial vertical bearing capacity using the superposition principle (Terzaghi 1951). The effects of load inclination and eccentricity are considered by introducing the load inclination factor and the effective foundation area (e.g. DNV 2016). The failure envelope method has been recommended as an alternative to conventional theories in some geotechnical design guidelines, such as ISO (2016). Current studies of the failure envelope method have been primarily confined to a single layer soil with a uniform or linearly increasing undrained shear strength profile (e.g. Bransby and Randolph 1998; Gourvenec and Randolph 2003). However, onshore clay deposits often have a thin layer of stiff crust with a relatively high undrained shear strength, which strongly affects the stability analysis of shallow foundations and embankments (Nakase et al. 1978).

The object of this paper is to investigate the undrained VHMT failure envelope of circular foundations founded on a surficial crust underlain by a uniform soil under a zero-tension interface condition using finite element analysis. An analytical expression for the failure envelope under combined VHMT loadings is derived in this paper.

Method – finite element analysis

A linear elastic perfectly plastic constitutive relationship with a Mohr-Coulomb (M-C) failure criterion was used to model the soil behavior. For undrained soil conditions, the M-C criterion degenerates to the Tresca criterion. Two fundamental parameters may affect the foundation

bearing capacity: the averaged undrained shear strength of the surficial crust layer, s_{ut}, and the crust thickness, t_c. In this paper, the ratio, $s_{\mathrm{u0}}/s_{\mathrm{ut}}$ (s_{u0} refers to the undrained shear strength of the underlying soil), has been varied from 0.2 to 1.0 (i.e. 0.2, 0.4, 0.6, 0.8 and 1.0), to represent a typical range of soil profiles. In eastern Canada, the thickness of the upper crust is often of the order of 3 m (Lefebvre et al. 1987). Typically, the diameter (*D*) of an onshore wind turbine foundation is very large (>15 m), and a diameter of 19 m is used, representing the typical dimension for current wind turbines in Canada. Therefore, this study has considered models with t_c/D ranging from 0.1 to 0.3 (i.e. 0.1, 0.2 and 0.3) to span most cases of practical interest.

In the analysis, s_{u0} was held constant at 100 kPa and the Poisson's ratio of the undrained soils was taken to be 0.49. Since the soil Young's modulus, E_{u}, does not influence the calculated collapse loads, a sufficiently large $E_{\mathrm{u}}/s_{\mathrm{u0}}$ ratio equal to 10000 was selected to minimize mesh distortion. The foundation was assumed to be a rigid body. A load reference point was used to apply prescribed displacements or loads, located at the bottom center of the foundation. A zero-tension, rough base is modelled using a Coulomb model with a friction coefficient of 20 (Shen et al. 2016). Probe tests and swipe tests were employed to detect the failure envelopes under various load conditions (Gourvenec and Randolph 2003).

The analysis in this paper was conducted using the finite element software ABAQUS (Dassault Systèmes 2016). To avoid the effects of model boundaries, the mesh length, *L*, and mesh height, *H*, were taken as 120 m and 50 m, following the recommendations of Deshpande (2016). A mesh convergence study was carried out for a number of cases, and a mesh composed of approximately 36000 8-noded brick elements (i.e. first-order, ABAQUS C3D8R) was selected, as shown in Fig. 1 (half-model). The cylindrical circumference of the soil was constrained to prevent out-of-plane translations and the bottom of the soil was fixed in the three orthogonal directions.

Fig. 1. Half-view of the FE mesh

Finite element results

Pure uniaxial capacities

The ultimate loads for vertical, horizontal and torsional modes are referred to as the corresponding uniaxial load-carrying capacities in the absence of the other loading modes. For zero-tension interface conditions, the ultimate moment capacity is represented by the maximum moment load under vertical loading only (Shen et al. 2016).

Since the uniaxial horizontal and torsional capacities of a surface foundation are purely related to the undrained shear strength of the surface soil: $H_{\mathrm{ult}} = As_{\mathrm{ut}}$ and $T_{\mathrm{ult}} = ADs_{\mathrm{ut}}/3$ (He and Newson 2020), only the vertical and moment capacities have been investigated. A crust correction factor, s_{cr}, defined as the ratio of the dimensionless capacity for a crusted soil to that of a uniform soil, is introduced to characterize the effect of a surficial crust:

$$s_{cr} = \frac{N_{s_{\mathrm{u0}}/s_{\mathrm{ut}}}}{N_{s_{\mathrm{u0}}/s_{\mathrm{ut}}=1}} \tag{1}$$

where $N^{v}_{s_{\mathrm{u0}}/s_{\mathrm{ut}}} = \frac{V_{\mathrm{ult}}}{A \cdot s_{\mathrm{ut}}}$ for the vertical capacity and $N^{m}_{s_{\mathrm{u0}}/s_{\mathrm{ut}}} = \frac{M_{\mathrm{ult}}}{A \cdot D \cdot s_{\mathrm{ut}}}$ for the moment capacity.

The variations of s_{crV} and s_{crM} with regard to $s_{\mathrm{u0}}/s_{\mathrm{ut}}$ and t_c/D are shown in Fig. 2, and a quadratic polynomial equation is proposed to estimate the relationships:

$$s_{cr} = f \cdot \left(\frac{s_{\mathrm{u0}}}{s_{\mathrm{ut}}}\right)^2 + 1.3\left(\frac{s_{\mathrm{u0}}}{s_{\mathrm{ut}}}\right) - [f + 0.3] \tag{2}$$

The coefficient, *f*, is a function of t_c/D, defined as $f(t_c/D) = -0.97t_c/D - 0.27$ for the vertical capacity and $f(t_c/D) = \frac{-1.18t_c/D}{t_c/D + 0.18}$ for the moment capacity.

Fig. 2. Crust correction factors of uniaxial capacities: (a) V_{ult} and (b) M_{ult}

H-V, M-V, T-V, M-H, H-T, M-T loading conditions

The normalized *H-V*, *M-V* and *T-V* failure envelopes with the corresponding uniaxial ultimate capacities for the cases of $s_{\text{u0}}/s_{\text{ut}} = 0.2 \sim 1.0$ and $t_c/D = 0.1 \sim 0.3$ are fitted using Eq. (3). Note that the dependence of *H-V*, *M-V* and *T-V* failure envelopes on $s_{\text{u0}}/s_{\text{ut}}$ and t_c/D is minor, and thus unique expressions are employed without the effects of $s_{\text{u0}}/s_{\text{ut}}$ and t_c/D.

$$\begin{aligned} V/V_{\text{ult}} &= 0.5 + 0.5\sqrt{1 - H/H_{\text{ult}}}, \text{ for } V/V_{\text{ult}} \geq 0.50 \\ H/H_{\text{ult}} &= 1, \text{ for } V/V_{\text{ult}} < 0.50 \end{aligned} \quad \text{(3a)}$$

$$M/M_{\text{ult}} = 4\left[V/V_{\text{ult}} - \left(V/V_{\text{ult}}\right)^2\right] \quad \text{(3b)}$$

$$\begin{aligned} V/V_{\text{ult}} &= 0.5 + 0.5\left[1 - \left(T/T_{\text{ult}}\right)^{2.5}\right]^{0.3}, \ V/V_{\text{ult}} > 0.50 \\ T/T_{\text{ult}} &= 1, \ V/V_{\text{ult}} \leq 0.50 \end{aligned} \quad \text{(3c)}$$

The *M-H, H-T, M-T* failure envelopes are obtained at $V/V_{\text{ult}} = 0.25$, 0.50 and 0.75. The dependence of *M-H, H-T, M-T* failure envelopes on $s_{\text{u0}}/s_{\text{ut}}$, t_c/D and V/V_{ult} levels is eliminated by normalizing the failure envelopes by their corresponding maximum values (i.e., H_{max}, M_{max} and T_{max}). Thus, unique equations are used to fit the failure envelopes, as shown by Eq. (4).

$$\left(H/H_{\text{max}}\right)^{2.0} + \left(M/M_{\text{max}}\right)^{1.6} = 1 \quad \text{(4a)}$$

(4b) $$\left(H/H_{\max}\right)^{1.5} + \left(T/T_{\max}\right)^{1.95} = 1$$

(4c) $$\left(M/M_{\max}\right)^{2.0} + \left(T/T_{\max}\right)^{2.0} = 1$$

Failure envelopes under combined VHMT loadings

Three sets of notation are now defined: (1) V_{ult}, H_{ult}, M_{ult}, T_{ult} – uniaxial ultimate capacity; (2) $H_{\max}$, $M_{\max}$, $T_{\max}$ – maximum capacity at a given level of the vertical load without other load components; (3) $H'_{\max}$, $M'_{\max}$ – reduced maximum capacity at a given level of the vertical load with a non-zero torsional load ($T \neq 0$).

Based on the above notation and the forms of equation used in the previous section, the general forms of the calculated envelopes are summarized in Eqs. (5) to (7). f_h, f_m and f_t are functions of the vertical load level. Specific expressions for these failure envelopes can be found in the previous section.

(5) $$\frac{H_{\max}}{H_{\text{ult}}} = f_h\left(\frac{V}{V_{\text{ult}}}\right),\ \frac{M_{\max}}{M_{\text{ult}}} = f_m\left(\frac{V}{V_{\text{ult}}}\right),\ \frac{T_{\max}}{T_{\text{ult}}} = f_t\left(\frac{V}{V_{\text{ult}}}\right)$$

(6) $$\left(\frac{H}{H_{\max}}\right)^a + \left(\frac{M}{M_{\max}}\right)^b = 1$$

(7) $$\left(\frac{H'_{\max}}{H_{\max}}\right)^c + \left(\frac{T}{T_{\max}}\right)^d = 1,\ \left(\frac{M'_{\max}}{M_{\max}}\right)^e + \left(\frac{T}{T_{\max}}\right)^f = 1$$

Eq. (6), which describes the *M-H* failure envelope under the condition of $T = 0$, is taken as the basic function. To derive the final VHMT envelope expression, a more generalized equation for the *M-H* failure envelope under the condition of $T \neq 0$ is required. Due to the very similar shape of the *M-H* failure envelope (only the sizes are different), it is reasonable to assume that under the condition of $T \neq 0$, Eq. (6) is still applicable for the *M-H* failure envelope normalized by the

131 corresponding maximum values, $H'_{\max}$ and $M'_{\max}$ (reduce to $H_{\max}$ and $M_{\max}$ in Eq. (6) if $T = 0$).
132 Therefore, Eq. (6) is replaced by a more generalized form:

133 (8) $$\left(\frac{H}{H'_{\max}}\right)^a + \left(\frac{M}{M'_{\max}}\right)^b = 1$$

134 Mathematical manipulations of Eqs. (5), (7) and (8) allow the formulation of an analytical
135 expression for the failure envelope in VHMT loading space in terms of V/V_{ult}, H/H_{ult}, M/M_{ult} and
136 T/T_{ult}:

137 (9) $$f\left(\frac{V}{V_{\text{ult}}},\frac{H}{H_{\text{ult}}},\frac{M}{M_{\text{ult}}},\frac{T}{T_{\text{ult}}}\right) = \left(\frac{H/H_{\text{ult}}}{\left[1-\left(\frac{T/T_{\text{ult}}}{f_t\left(V/V_{\text{ult}}\right)}\right)^d\right]^{\frac{1}{c}} \cdot f_h\left(V/V_{\text{ult}}\right)}\right)^a + \left(\frac{M/M_{\text{ult}}}{\left[1-\left(\frac{T/T_{\text{ult}}}{f_t\left(V/V_{\text{ult}}\right)}\right)^f\right]^{\frac{1}{e}} \cdot f_m\left(V/V_{\text{ult}}\right)}\right)^b = 1$$

138 In practical design, the design loads (factored loads and materials), VHMT, can be directly
139 substituted into the left-hand side of Eq. (9); values less than 1 represent a sufficient ultimate limit
140 design and vice versa.

141 As an example, the expression of the VHMT failure envelope for the case of $s_{\text{u0}}/s_{\text{ut}} = 0.6$ and t_c/D
142 $= 0.2$ is presented. To visualize the shape of the 4-D failure surface, three 3-D failure surfaces in
143 terms of V/V_{ult}, H/H_{ult}, M/M_{ult} and T/T_{ult} are presented in Fig. 3. The specific curves obtained
144 from the FE results in the previous section are also incorporated for comparison. For the VHT and
145 VMT failure surfaces, the portion of $T < 0$ is also incorporated due to the symmetry about the
146 plane of $T = 0$.

147 **Fig. 3.** 3-D failure surfaces for the case of $s_{\text{u0}}/s_{\text{ut}} = 0.6$ and $t_c/D = 0.2$: (a) VHM at $T = 0$; (b)
148 VHT at $M = 0$ and (c) VMT at $H = 0$

Conclusions

The VHMT failure envelopes of circular foundations resting on a stiff crust which overlies the main soil deposit under undrained conditions have been studied using FE analysis. A zero-tension interface and undrained soil conditions were considered. Cases with five values of s_{u0}/s_{ut} and three values of t_c/D have been ultilized to derive the analytical expression for the VHMT failure envelope. These approaches should aid the assessment of the ultimate capacity of shallow circular foundations under complex loading conditions.

Acknowledgements

The authors would like to acknowledge the financial support of Natural Sciences and Engineering Research Council (Grant No.: RGPIN-2015-06062). The first author is grateful for the financial support of the China Scholarship Council (CSC).

References

Bransby, M.F., and Randolph, M.F. 1998. Combined loading of skirted foundations. Géotechnique, **48**(5): 637-655.

Dassault Systèmes 2016. Abaqus analysis user's manual. Simulia Corp., Providence, RI, USA.

Deshpande, V.M. 2016. Numerical Modelling of Wind Turbine Foundations subjected to Combined Loading. M.Sc. thesis, Department of Civil and Environmental Engineering, The University of Western Ontario, London, Ont.

DNV, GL, DNVGL-ST-0126 2016. Support structures for wind turbines. DNV GL, Oslo, Norway.

168 Gourvenec, S., and Randolph, M. 2003. Effect of strength non-homogeneity on the shape of failure
169 envelopes for combined loading of strip and circular foundations on clay. Géotechnique, **53**(6):
170 575-586.

171 He, P., and Newson, T. 2020. Undrained capacity of circular foundations under combined
172 horizontal and torsional loads. Géotechnique Letters, 10(2): 186-190.

173 ISO (International Standards Organisation) 2016. Petroleum and natural gas industries specific
174 requirements for offshore structures -- part 4: geotechnical and foundation design considerations,
175 2nd edition. International Standards Organisation, Geneva, Switzerland.

176 Lefebvre, G., Paré, J.J., and Dascal, O. 1987. Undrained shear strength in the surficial weathered
177 crust. Canadian Geotechnical Journal, **24**(1): 23-34.

178 Nakase, A., Kimura, T., Saitoh, K., Takemora, J., and Hagiwara, T. 1978. Behavior of Soft Clay
179 with a Surface Crust. *In* Proceedings of the eighth Asian Regional Conference on Soil Mechanics
180 and Foundation Engineering, Kyoto, Japan, 20-24 July 1987. Japanese Society of Soil Mechanics
181 and Foundation Engineering, Tokyo, **1**: pp. 410-414.

182 Shen, Z., Feng, X., and Gourvenec, S. 2016. Undrained capacity of surface foundations with zero-
183 tension interface under planar VHM loading. Computers and Geotechnics, **73**: 47-57.

184 Terzaghi, K. 1951. Theoretical soil mechanics. John Wiley & Sons, Inc., Hoboken, N.J.

185 **List of Figures**

186 **Fig. 1.** Half-view of the FE mesh

187 **Fig. 2.** Crust correction factors of uniaxial capacities: (a) V_{ult} and (b) M_{ult}

188 **Fig. 3.** 3-D failure surfaces for the case of $s_{\mathrm{u0}}/s_{\mathrm{ut}} = 0.6$ and $t_c/D = 0.2$: (a) VHM at $T = 0$; (b)

189 VHT at $M = 0$ and (c) VMT at $H = 0$

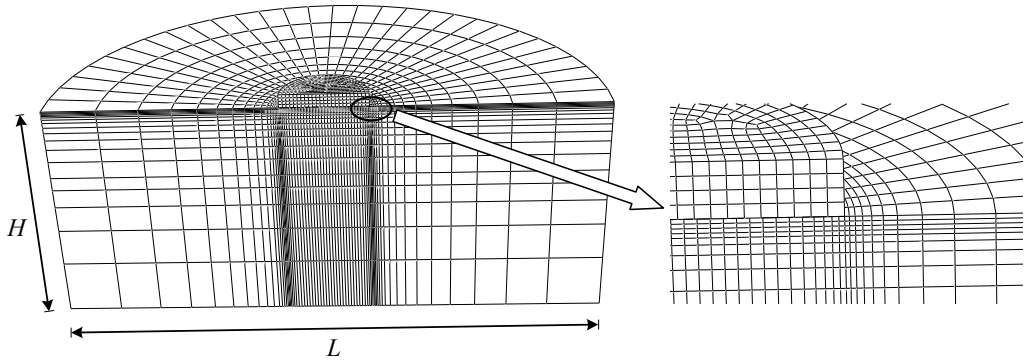

Fig. 1. Half-view of the FE mesh

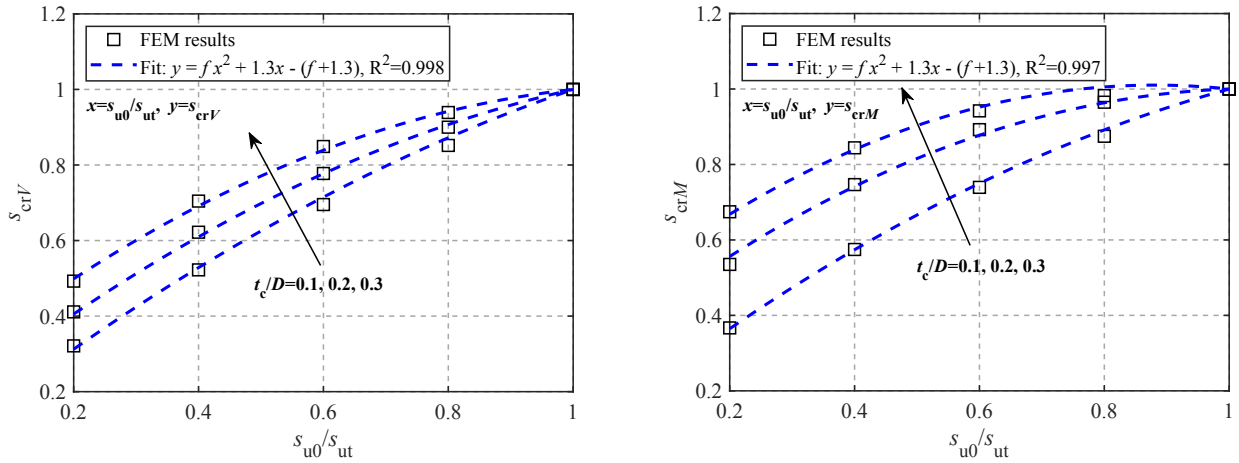

(a) V_{ult} (b) M_{ult}

Fig. 2. Crust correction factors of uniaxial capacities: (a) V_{ult} and (b) M_{ult}

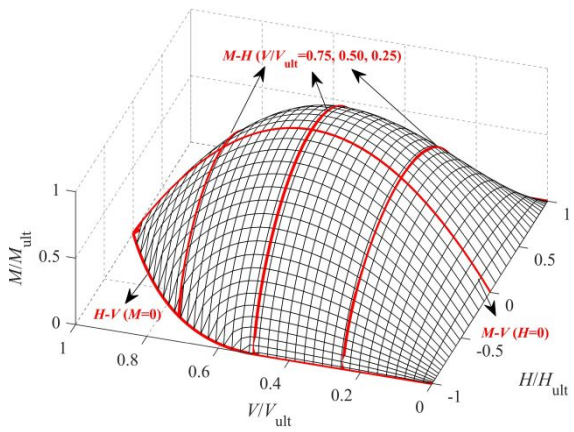

(a) VHM at $T = 0$

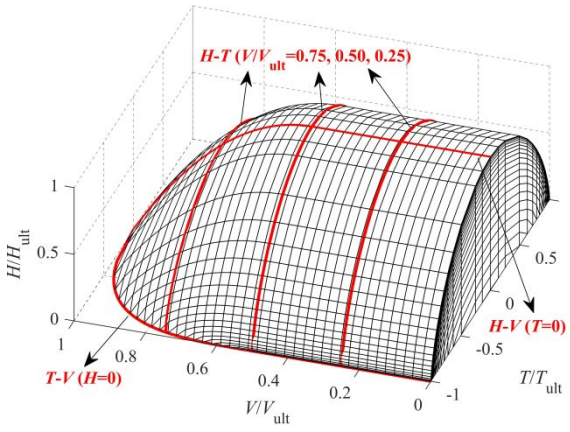

(b) VHT at $M = 0$

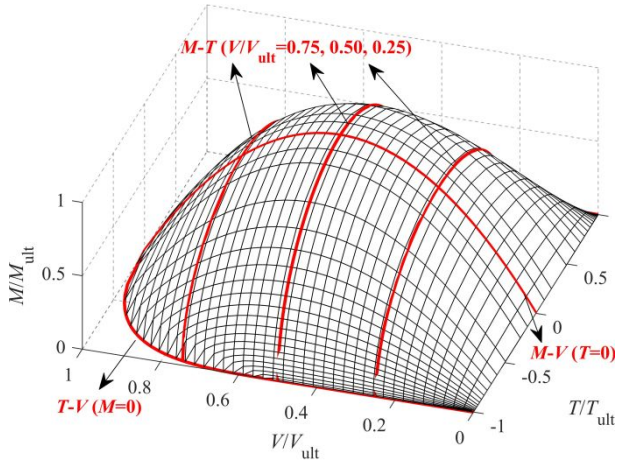

(c) VMT at $H = 0$

Fig. 3. 3-D failure surfaces for the case of $s_{u0}/s_{ut} = 0.6$ and $t_c/D = 0.2$: (a) VHM at $T = 0$; (b) VHT at $M = 0$ and (c) VMT at $H = 0$